Dynamical properties of a frustrated monolayer of Ar on MgO(100): A neutron-scattering study

J. M. Layet, M. Bienfait
Faculté des Sciences de Luminy, Case 913, 13288 Marseille Cedex 9, France

C. Ramseyer, P. N. M. Hoang, C. Girardet
Laboratoire de Physique Moléculaire, Université de Franche Comté, 25030 Besançon Cedex, France

G. Coddens
Laboratoire Léon Brillouin, CE-Saclay, 91191 Gif-sur-Yvette Cedex, France
(Received 7 December 1992; revised manuscript received 25 March 1993)

The paper reports quasielastic and inelastic neutron-scattering (INS) measurements on both the 2×3 commensurate solid and the hexagonal incommensurate structure of monolayer Ar adsorbed on MgO(100). The principal findings are (1) there is reasonable agreement between INS spectra and those calculated for the two phases and (2) there is a liquidlike mobility in the unidirectional disordered phase which results from heating the 2×3 commensurate solid.

I. INTRODUCTION

The structure of adsorbed monolayers results from the interplay between the symmetries of both adsorbate and substrate and the corrugation potential of the surface.[1,2] According to the nature and periodicity of the various forces, the adsorbed solid can be commensurate, incommensurate, or partly in register with the substrate. Of particular interest is the case where the balance between forces is so delicate that any slight change in chemical potential (or concentration) modifies the adsorbed structure drastically. A typical example is the adsorption of Ar on MgO(100). In that system the difference between the square symmetry of the substrate and the hexagonal "natural" packing of the adsorbed monolayer induces a frustration which is resolved by a subtle competition between the various interaction energies involved in the substrate and the adsorbate.

Previous experimental and theoretical studies[3–5] have demonstrated that the Ar monolayer structure changes with increasing concentration (or chemical potential). At intermediate coverage and low temperature ($T \leq 35$ K), the solid overlayer is a 2×3 commensurate phase, which becomes a 2×4 structure at coverage close to unity, finally reaching a hexagonal close-packed structure at the beginning of the second layer condensation. In the rectangular 2×3 solid [Fig. 1(a)], the Ar atoms are organized in rows parallel to the Mg[110] troughs of the MgO(100) surface. In the hexagonal phase [Fig. 1(b)], all the atoms are out of registry. Above 40 K, the 2×3 structure loses its long-range order in one direction only, whereas the hexagonal packing remains stable up to 55 K. This structural information has been obtained by both electron- and neutron-diffraction measurements. In particular, neutron diffraction[5] has shown that a strongly anisotropic uniaxial disorder occurs above 40 K for the 2×3 structure in the direction parallel to the troughs, but cannot determine whether it is static or dynamic.

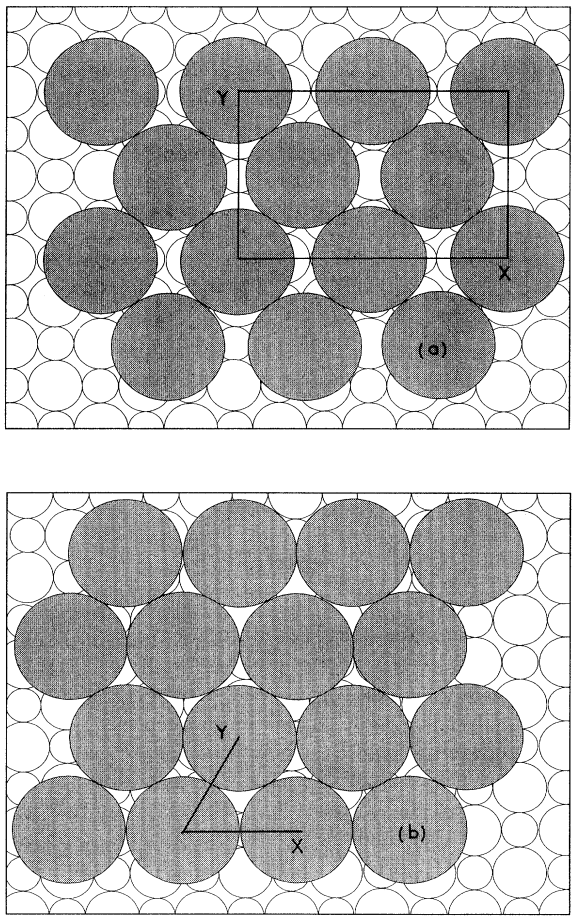

FIG. 1. The low-temperature (10 K) structures of Ar overlayer adsorbed on MgO(100). (a) The partially commensurate rectangular 2×3 solid at intermediate coverages (0.7–0.95 layer); (b) the hexagonal close-packed structure at monolayer completion.

The aim of this work is to improve our knowledge of the Ar/MgO interaction potential through a comparison between calculations and experiments. First, quasielastic neutron-scattering (QENS) experiments, a technique well-suited for mobility measurements,[6,7] have been performed to measure the mobility within the unidirectional disordered 2×3 structure which, for simplicity, will be labeled $2 \times \infty$ in the following. As stated above, the low-temperature 2×3 or hexagonal structures result from a delicate balance between the lateral Ar-Ar forces, the adsorbate-substrate interactions, and the imposed chemical potential. In particular, the corrugation potential of the MgO surface is not known accurately but it can be reached indirectly through the measurement of the layer mobility from the QENS. Secondly, a measurement of the phonon density of states by inelastic neutron scattering (INS) should provide an easy way to test the quality of the Ar/MgO interaction potential. It has been shown by lattice-dynamics calculations[8,9] that (i) some phonon modes of the 2×3 structure are very sensitive to the potential through its second derivatives, which determine the force constants, and (ii) the vibrational spectrum depends strongly on the adsorbate packing (2×3 or hexagonal). At low temperature, as shown in Sec. II, the measurable energy transfers for the adsorbate phonons lie in the 1–10-meV range. Consequently, the coherent inelastic neutron-scattering function[10,11] is well adapted to the interpretation of the low-temperature (10 K) inelastic-scattering spectra. But, at higher temperature (45 K), where some mobility is expected within the $2 \times \infty$ overlayer, this is no longer valid. The kinetic energy of the moving atoms usually ranges between 0 and 0.5 meV and it has been demonstrated that, at small energy transfers,[12,13] the scattering function exhibits wings whose widths are proportional to the translational diffusion coefficient D of the moving atoms. Previous measurements[14] performed on bulk liquid argon have shown that the full width at half maximum (FWHM) ΔE is given, at small scattering vector $\mathbf{Q}$ ($Q < 1.5$ Å^{-1}), by the following expression:

$$\Delta E \sim 2\hbar D Q^2. \tag{1}$$

We will use this equation to derive the diffusion coefficient from the data obtained at 45 K for small energy transfers. Hence, the QENS technique allows us to measure the energy broadening resulting from the interaction of neutrons with mobile atoms or molecules.[15]

After reporting and discussing the QENS and INS experiments in Sec. II, we calculate the diffusion coefficient for the adsorbed monolayer and the corresponding INS spectrum deduced from lattice-dynamics calculations in Sec. III. Finally in Sec. IV, these results are tested against experimental data.

II. EXPERIMENTAL

A. General

As stated in the Introduction, the use of uniform powders in surface studies by neutron scattering is useful to increase the surface-to-bulk ratio because neutrons penetrate condensed matter easily and are usually not sensitive to surfaces. Here the experiment was carried out on sintered powders of MgO cubes[16] having a specific area of 13 m^2/cm^3. These sintered pills have been used in three preceding studies.[17–19] The sample was processed as indicated in Ref. 16.

An adsorption isotherm measurement was carried out at 77.3 K using Ar to calibrate the monolayer coverage. Coverage 1 is set at the inflection point between the first and second step (first and second adsorbed layer). The sample has a total area of about 200 m^2 and a weight of about 36 g. The experiments were carried out on the Mibemol spectrometer at Laboratoire Léon Brillouin–Saclay for two argon coverages, 0.8 and 1.16 atomic layers, and at two temperatures, 10 and 45 K, i.e., below and above the 2×3 unidirectional disordered phase in the submonolayer range. The gas was adsorbed at $\sim$ 73 K. Then the sample was slowly cooled down to the temperature at which the layer reorganizes. The 10-K experiment was aimed at measuring the phonon density of states in the Ar layer. The incident energy $E_0 = 7$ meV ($\lambda_0 = 3.42$ Å) was suitable for INS measurements. The corresponding resolution was triangular shaped and has a FWHM of 0.3 meV for an energy loss of 4 meV. Twelve detector banks were used at various scattering vectors $\mathbf{Q}$ ranging from 0.56 to 3.37 Å^{-1}. The 45-K experiment, on the other hand, was mainly devoted to mobility measurements in the phases stable at this temperature for the 0.8 and 1.16 coverages. The selected incident energy $E_0 = 1.28$ meV ($\lambda = 8$ Å) was suited to QENS studies.[17–19] At small energy transfers (< 0.5 meV) the Mibemol resolution was 0.05 meV; it becomes poorer (0.3 meV) for energy gains close to 4 meV; the $\mathbf{Q}$ range of the 12 detector banks was 0.37 to 1.44 Å^{-1}. The scattering spectra were obtained by subtracting the background due to the cell and to the bare MgO pills.

Two runs have also been performed at the Institut Laüe Langevin (Grenoble) on the IN5 instrument[20] using an incident energy $E_0 = 15.5$ meV ($\lambda = 2.3$ Å) and a resolution of about 1 meV for a neutron energy gain of 5 meV, on the same sample with argon coverage of 0.8 layer. The first was carried out at 10 K and the second at 45 K. The recorded spectra showed energy losses below 5 meV at 10 K and very substantial broadening at 45 K. These results allowed us to select the energy range (and resolution) required to carry out more complete studies on the Mibemol spectrometer.

B. Quasielastic neutron scattering by the Ar layer at 45 K

As stated above, the 2×3 solid, stable at low T in the submonolayer range, undergoes a transition at about 40 K toward a unidirectional disordered phase. QENS at 45 K was used to determine whether this disorder is static or dynamic and to measure the translational mobility, if any. Previous diffraction results[5] have shown that the long-range order can be restored at the same temperature (45 K) by increasing the coverage. At mono-

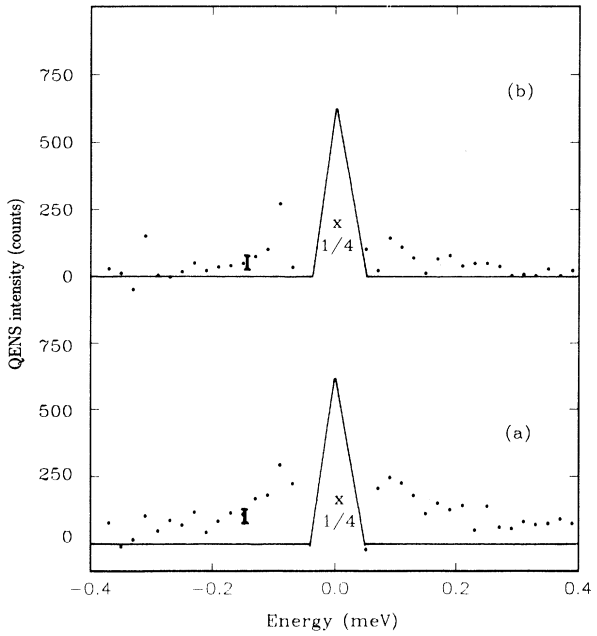

FIG. 2. Quasielastic neutron-scattering spectra of ^{36}Ar/MgO(100) at 45 K. Counts are plotted vs the energy; the vertical bars represent the experimental errors. (a) At 0.8 layer, the wings are a clear signature of the existence of a liquid-like phase. (b) At 1.16 layer, the wings disappear and the layer is solidified. The triangle represents the experimental line shape reduced by a factor of 1/4.

layer completion, the Ar film becomes a hexagonal solid. The results are shown in Fig. 2 for an incident energy $E_0 = 1.28$ meV ($\lambda = 8$ Å). They cover the whole wave-vector transfer range between 0.53 and 1.28 Å^{-1}. The observation at 0.8 layer and 45 K of nearly symmetric wings having a width of several hundred μeV [Fig. 2(a)] is a clear signature of the existence of a liquidlike mobility within the adsorbed layer. These wings disappear almost completely at larger coverage [1.16 layer, Fig. 2(b)] indicating a solidification of the film. The remaining very small wings may be attributed to the existence of a fluid fraction (0.16 layer) located above the hexagonal solid monolayer. The data recorded for 0.8 layer at 45 K can be analyzed quantitatively using Eq. (1). Although the experimental scattering data were collected for 24 h for each physical condition (coverage and temperature), the statistics are not very good, as seen in Fig. 2. Hence, only an estimate of the diffusion coefficient D can be obtained from the widths ΔE recorded at different scattering vectors. The QENS spectra were assumed to be Lorentzian with a width given by Eq. (1). These Lorentzian curves were convoluted with the instrumental resolution and fitted to the experimental results. The value of D at 45 K for the $2 \times \infty$ phase is about $3 \pm 1 \times 10^{-5}$ cm^2 s^{-1}. Hence the film is highly mobile, although some Ar long-range order persists in the direction perpendicular to the [110] channels of the MgO(100) surface. The statistics of the data are too poor to test more elaborate models of diffusion, although an anisotropic two-dimensional mobility is suggested by the diffraction data.

C. Inelastic neutron-scattering by the Ar layer at 10 K and 45 K

The INS measurements are intended to record the phonon losses (or gains) for the different structures stable at 0.8 and 1.16 layers at 10 and 45 K and to compare the spectra with those determined by lattice-dynamics calculations. At 10 K, the incident neutron energy (7 meV, $\lambda = 3.42$ Å) was adapted to the measurements of the maximum of the phonon density of states observed at about 4 meV in the preliminary experiment.[20] The inelastic-scattering data for 1.16 layer (hexagonal structure) and 0.8 layer (2×3 structure) are represented in Figs. 3(a) and 4(a), respectively. These spectra correspond to the summation of the whole set of the 12 detector banks ranging from $Q = 0.56$ to $Q = 3.37$ Å^{-1}. At 1.16 layer and 10 K, the loss spectrum exhibits a broad peak at about −4 meV and a plateau between −3 and −2 meV, whereas the gain side has a small component decreasing with energy. At 0.8 layer and 10 K, the peak at about −4 meV is shifted to a lower energy and two new broad peaks occur at about −2 and −1.5 meV. The hexagonal solid has a higher density of phonon states

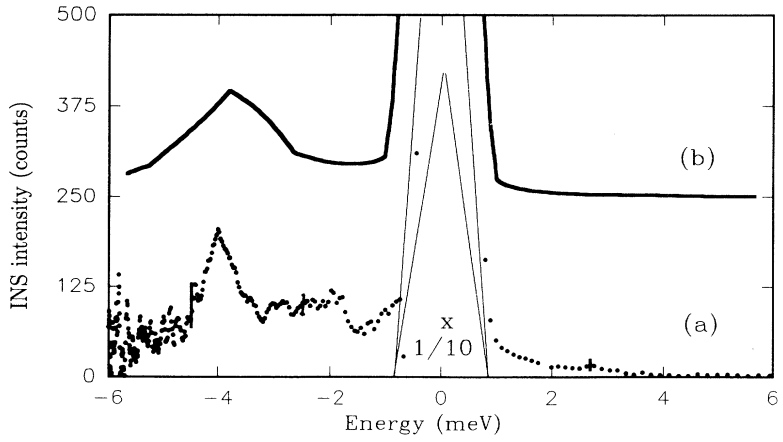

FIG. 3. Inelastic neutron-scattering spectra of ^{36}Ar/MgO(100) at 10 K. (a) Experimental spectra at incident energy of 7 meV for a 1.16 layer (hexagonal structure); the vertical bars and the triangle represent experimental errors and the experimental broadening (reduced by a factor of 1/10), respectively; (b) calculated spectrum for the hexagonal incommensurate structure after convoluting with the instrumental line shape of 0.3 meV at a neutron gain of 5 meV (see text). Units are arbitrary and the baseline is shifted with respect to curve (a).

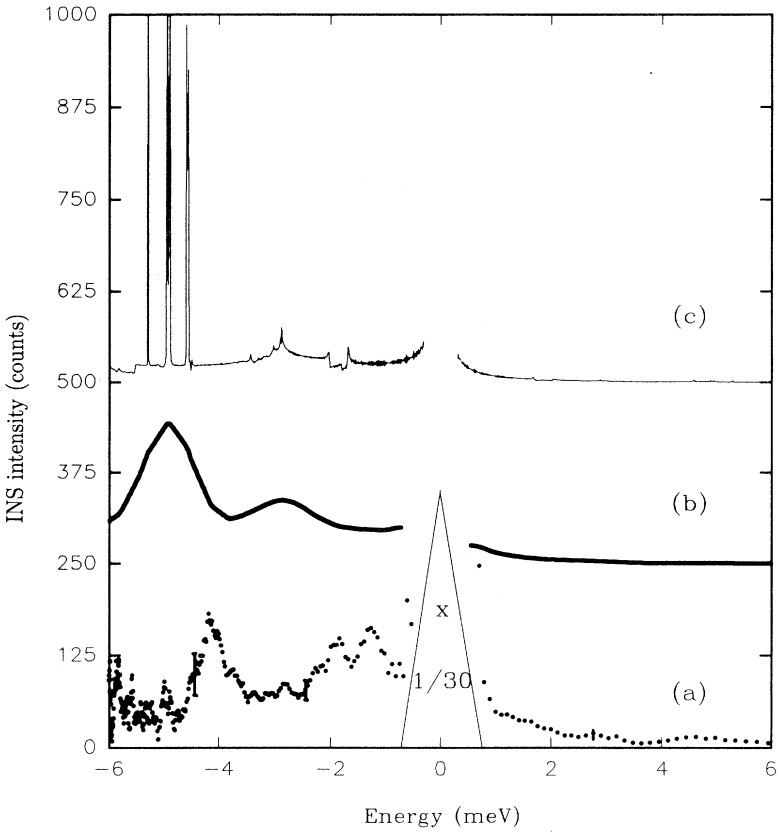

FIG. 4. Inelastic neutron-scattering spectra of ^{36}Ar/MgO(100) at 10 K. (a) Experimental spectra at incident energy of 7 meV for a 0.8 layer 2×3 structure; note the difference between the experimental errors (vertical bars) in the gain and the loss energy ranges; the triangle represents the experimental line shape reduced by a factor of 1/30. (b) Calculated spectrum for the 2×3 structure, in arbitrary units, after convoluting with the instrumental resolution of 0.3 meV at a neutron gain of 5 meV (see text). (c) Calculated spectrum without broadening. The width of the peaks is due to the numerical step in the calculation of the dispersion branches. Baselines of curves (b) and (c) are shifted with respect to curve (a).

than the 2×3 structure between -3 and -4 meV and a lower density between -2 and -1 meV.

As explained in Sec. II, the neutron experiment performed at 45 K was mainly intended to measure by QENS the mobility in the $2 \times \infty$ unidirectionally disordered structure and the incident energy (1.28 meV) and resolution (0.05 meV) were selected for this purpose. This experiment, however, also provided information on the vibrational states of the adsorbate from measurements of the INS spectra on the energy-gain side, but with a poorer resolution. The spectra recorded at 45 K, 0.53 $\text{Å}^{-1} < Q < 1.28$ Å^{-1}, for 1.16 and 0.8 layers are represented in Figs. 5(a) and 6(a), respectively. They both exhibit a broad component and a superimposed peak at about 4 meV. The intensity of the peak is smaller for the $2 \times \infty$ structure [Fig. 6(a)] than for the hexagonal packing [Fig. 5(a)]. The features of Figs. 5 and 6 will be interpreted in Sec. III.

III. THEORETICAL

A. Monolayer dynamics

The geometries of the 2×3 and the hexagonal Ar monolayers (Fig. 1) have been determined within the rigid,

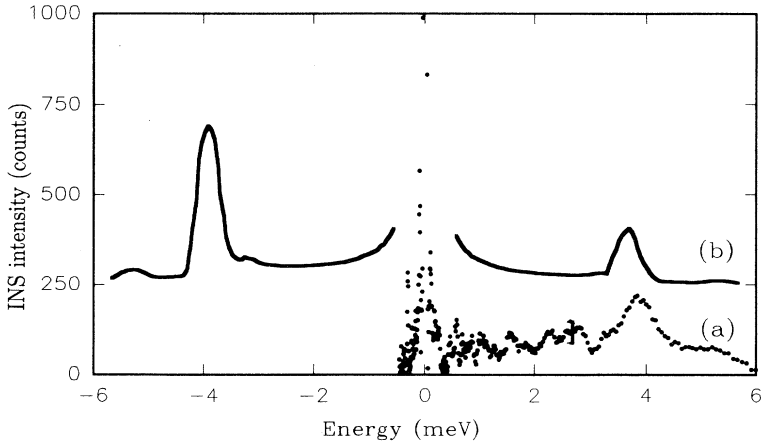

FIG. 5. Inelastic neutron-scattering spectra at 45 K. (a) Gain spectrum recorded at 1.16 layer (hexagonal structure) with an incident energy 1.28 meV. (b) Calculated spectrum in arbitrary units for the hexagonal incommensurate structure with the instrumental resolution of 0.3 meV at a neutron gain of 5 meV (see text). The baseline of curve (b) is shifted with respect to curve (a).

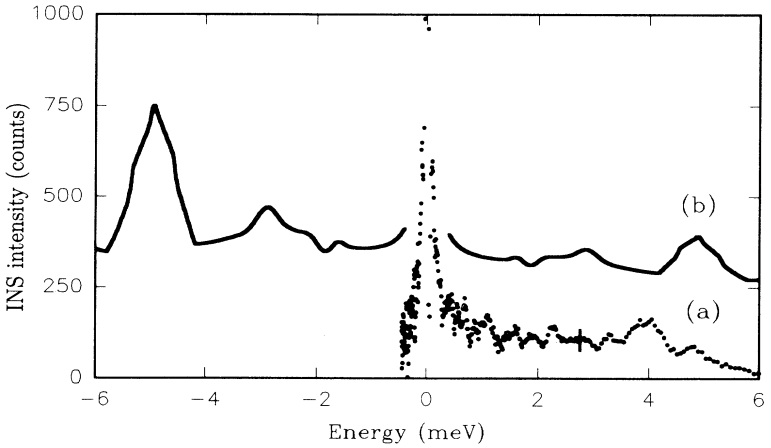

FIG. 6. Inelastic neutron-scattering spectra at 45 K. (a) Gain spectrum recorded at 0.8 layer [uniaxially disordered phase ($2 \times \infty$ structure)] with an incident energy of 1.28 meV. (b) Calculated spectrum in arbitrary units for the $2\times\infty$ structure after convoluting with the instrumental linewidth of 0.3 meV and at a neutron gain of 5 meV (see text). The baseline of curve (b) is shifted with respect to curve (a).

undistorted substrate approximation by minimizing the total interaction potential which is a sum of the intralayer and layer-substrate potentials.[9] The dominant contribution to these two potentials is the dispersion-repulsion term represented by an atom-atom Lennard-Jones (LJ) potential. Additional contributions[4] such as those arising from the polarization of Ar atoms by the electrostatic field of the substrate, the three-body and the substrate-mediated interactions, and the rumpling of the MgO surfaces are not considered. These contributions are not only small but also time consuming in the computation of the equilibrium structure of the monolayer.

Within these approximations, the monolayer dynamics are studied by diagonalizing the dynamical matrix with components $(\alpha, \beta = x, y, z)$,

$$D_{\alpha\beta}(s, s', \mathbf{q}) = \frac{1}{M} \sum_{l,l'} e^{i\mathbf{q}\cdot\mathbf{R}(ll')} \left[\Phi^{M}_{\alpha\beta} \begin{pmatrix} l & l' \\ s & s' \end{pmatrix} + \Phi^{MS}_{\alpha\beta} \begin{pmatrix} l \\ s \end{pmatrix} \delta_{ll'} \delta_{ss'} \right]. \tag{2}$$

$\mathbf{q}$ defines the two-dimensional (2D) wave vector, and s and s' characterize two monolayer Ar atoms (mass M) pertaining to the l and l' cells at a distance $\mathbf{R}(ll')$. The force constant tensors Φ^{M} and Φ^{MS}, limited to the nearest and second-nearest neighbors and derived from the intramonolayer and layer-substrate potentials, are determined within a slightly modified harmonic model. In the pure harmonic model, the force constants are determined at the equilibrium configuration of the monolayer as a whole. Thus, some Ar sites are in register with the substrate and some are not. Consequently, the potential wells for these latter sites are not strictly harmonic, and this leads to small inaccuracies, mainly in the nondiagonal force-constant values. In order to take the anharmonicity of these wells into account, the corresponding mixed force constants have been replaced by averaged values. With this slight correction, the instabilities which occurred with the pure harmonic model[9] disappear but the pattern of the phonon-dispersion curves remains the same. The calculation of the frequencies $\omega_j(\mathbf{q})$ and eigenvectors $\mathbf{e}(s, \mathbf{q}, j)$ of the dynamical matrix $D(s, s', \mathbf{q})$ leading to the phonon dispersion curves are performed on a rank $12 = 4 \times 3$ matrix (four atoms with three degrees of freedom) for the 2×3 layer and on a rank $3 = 1\times3$ matrix for the hexagonal layer. In this latter case, the dispersion arising from the presence of the corrugated substrate is taken into account only in the perpendicular mode by determining the width of the frequency distribution of the layer atoms vibrating perpendicular to the substrate surface. The frequency density of the monolayer modes can then be easily calculated, as explained in Ref. 9.

B. Surface diffusion

The mobility of the 2×3 Ar monolayer is studied by considering the surface diffusion of the primitive cell containing four Ar atoms rigidly bonded together, along the x and y directions (Fig. 1). A transition-state model based on the transit time concept is used[21] to determine the diffusion constants D_x and D_y along the two perpendicular directions. The diffusion constant D_α along $\alpha = x$ or y is given by

$$D_\alpha = \bar{\lambda}^2 \, e^{-\beta[V(\alpha^{\max}) - V(\alpha^{\min}) + K(\alpha^{\max})]} \left[\sqrt{2\pi\beta m^*} \int_{\alpha_n^{\max}}^{\alpha_{n+1}^{\max}} d\alpha \, e^{-\beta[V(\alpha) - V(\alpha^{\min}) + K(\alpha)]} \right]^{-1}, \tag{3}$$

where $\bar{\lambda}$ defines the spatial period, equal to the lattice parameter a for this 2×3 structure, $\beta = (kT)^{-1}$, and m^* is the effective mass of the cell which takes into account the change of the cell to surface distance when the four atoms escape from a potential well to an adjacent one, within the rigid-cell approximation. V describes the potential experienced by the system for various positions α for which the extremum values are $\alpha^{\max}$ and $\alpha^{\min}$ and

the index n refers to the number of minimum wells. K is the usual free energy of the cell, determined within the present harmonic theory.[22]

C. Inelastic-scattering spectrum

The coherent-scattering function, per unit of outgoing energy and per unit of solid angle, for momentum and energy transfers $\hbar\mathbf{Q}$ and $\Delta E = \hbar\omega$ is written for the $(\mathbf{q}, j)$ monolayer phonon as[9–11]

$$\sigma(\mathbf{Q},\omega) = \frac{\hbar}{2M}\,\gamma_{\rm coh}^2\,\frac{(2\pi)^2}{S}\,\frac{k'_N}{k_N}\sum_{\mathbf{g}}\frac{|\,F_j(\mathbf{q})\,|^2}{\omega_j(\mathbf{q})}(n_{\mathbf{q}j}+\tfrac{1}{2}\mp\tfrac{1}{2})\delta[\Delta E\mp\hbar\omega_j(\mathbf{q})]\delta(\mathbf{Q}_{\|}+\mathbf{q}-\mathbf{g}), \tag{4}$$

where $\gamma_{\rm coh}$ is the average scattering length for neutrons with incident and scattered momentum $-\mathbf{k}_N$ and $\mathbf{k}'_N(\mathbf{Q}=\mathbf{k}_N-\mathbf{k}'_N)$; S and $\mathbf{g}$ define, respectively,[9] the area of the 2D primitive cell and the reciprocal vector for the adlayer (S_C, $\mathbf{g}_C$ for the commensurate structure and S_I, $\mathbf{g}_I$ for the incommensurate one). $n_{\mathbf{q}j}$ is the conventional Bose function for the $(\mathbf{q}, j)$ phonon and the two Dirac functions describe the energy and momentum conservation in the neutron-phonon collisional process. The inelastic structure factor $F_j(\mathbf{q})$ depends on the usual Debye-Waller and on the function $f_{ss'}$ defined as[9]

$$f_{ss'} = e_z(s,\mathbf{q},j)\;e_z^*(s',\mathbf{q},j)\left[\frac{\sin Qh_{ss'}}{Qh_{ss'}}\right]+\left(\mathbf{e}(s,\mathbf{q},j)\;\mathbf{e}^*(s',\mathbf{q},j)-3\;\frac{e_z(s,\mathbf{q},j)\;e_z^*(s',\mathbf{q},j)}{Q^2h_{ss'}^2}\right)\left[\frac{\sin Qh_{ss'}}{Qh_{ss'}}-\cos Qh_{ss'}\right], \tag{5}$$

where $h_{ss'} = h(s)-h(s')$ characterizes the relative height of the layer atoms above the substrate surface. When $s = s'$, the function f_{ss} reduces to $\frac{1}{3}$; this approximate form can be used for the hexagonal geometry. Note that Eq. (5) is obtained after averaging over the $\mathbf{Q}$-vector orientations, consistently with experiments on powders. Indeed in such experiments, all orientations of the incident neutron momentum occur, therefore an average over the orientation of the transferred momentum $\mathbf{Q}$ should be performed. The broadening process described by the time-correlation function, which takes into account the finite lifetime of phonons, is disregarded in Eq. (4). But the broadening of the experimental spectrum is simulated by convoluting the scattering function $\sigma(\mathbf{Q},\omega)$ by a triangular function which describes the instrumental line shape.

IV. COMPARISON BETWEEN EXPERIMENTAL AND THEORETICAL RESULTS

A. Monolayer mobility at 45 K

The QENS estimate of the diffusion constant for the Ar monolayer adsorbed on MgO(100) (Sec. II B) is now compared to the result given by the transition-state model. Along the x direction, the effective mass ratio m^*/m is 1.07 and the depth of the potential well is 9.6 meV. Equation (3) leads to the value $D_x = 1.65\times10^{-5}$ cm^2 sec^{-1} at $T = 45$ K, compared to the experimental fit of $3\pm1\times10^{-5}$ cm^2 sec^{-1}. The same calculation performed along the y direction gives $D_y = 2.5\times10^{-9}$ cm^2 sec^{-1}. This result clearly shows that the diffusion along y is hindered, in agreement with the experimental observation, indicating strong correlations in the y direction, i.e., perpendicular to the Mg troughs.

The diffusion constant D_α of an Ar atom which migrates in the second layer on top of the hexagonal incommensurate Ar monolayer adsorbed on MgO(100) has been calculated within the same model. The diffusion is assumed to be along the medians of the triangle formed by three nearest-neighbor Ar atoms which are equilibrium valleys. The calculated value is $D = 7.3\times10^{-5}$ cm^2 sec^{-1}, so the Ar diffusion in the second layer is easier by a factor of 4. Hence the observation of a remaining small and broad wing in the QENS spectra recorded at 45 K for the 1.16 layer [Fig. 2(b)] is consistent with the existence of a mobile fraction in the second adsorbed layer.

Note that the present transition-state model depends exponentially on the height of the potential well occurring in D_α. Therefore a measurement of D_α provides a fair estimate of the barrier height, i.e., of the corrugation along the diffusion path. For the experimental value $D = 3\times10^{-5}$ cm^2 sec^{-1}, the corrugation would be 7.3 meV.

B. Comparison of the inelastic-scattering spectra

The consideration of effective force constants mainly improves the dispersion curves with energies lower than 2 meV; the unphysical $\mathbf{q}$ gap at zero frequency and the anomalous behavior of two dispersion curves at large-$\mathbf{q}$ values due to anharmonicity disappear. The remaining dispersion scheme is not modified significantly and we refer to Refs. 9 and 23 for an examination of the dispersion branches of the 2×3 and hexagonal phases.

The theoretical INS spectrum without broadening for the 2×3 structure is presented in Fig. 4(c) at $T = 10$ K. The apparent broadening is only due to the $\mathbf{q}$ sampling of the dispersion curves and of the density of states which introduces a finite numerical width. The low-temperature spectrum is asymmetric as a consequence of the influence of the Bose factor in the phonon creation

or annihilation process in Eq. (4). The loss spectrum exhibits three main peaks at -4.5, -4.9, and -5.3 meV and additional structures at -2.9 meV and between -2 and -1 meV. The three peaks are due to the nondispersive perpendicular vibrations of the four monolayer atoms in the unit cell; two of them are equivalent. The low-energy structures characterize the quasiacoustic behavior of the dispersion branches since the layer adsorption in a commensurate phase breaks down the translational invariance and leads to frequency gaps for the two acoustic branches. As a result, these acoustic branches appear to be less dispersive in a significant range above zero q value and they give rise to an enhancement of the density of states at low-energy values.

The theoretical spectrum has been convoluted with the instrumental line shape for comparison with the experimental spectrum. Figure 4(b) shows the resulting broadened inelastic spectrum at $T = 10$ K. The three peaks in the bar spectrum are replaced by a structured band centered near -5 meV (loss spectrum) with an additional structureless band at about -2.9 meV. The FWHM of the main band is 1.2 meV. The comparison with the experimental spectrum [Fig. 4(a)] shows good agreement since the gain and/or loss intensity asymmetry is well reproduced as well as the shape of the bands. The noticeable difference is due to an overestimate of the phonon energy in the calculated spectrum, the experimental peaks being around -4.2 and -1.5 meV. The width of the main band, at about 1.5 meV, is close to the calculated value.

At $T = 45$ K, the INS spectrum has been calculated for two situations. The first corresponds to a hypothetical high-temperature 2×3 geometry after the unbroadened spectrum has been convoluted with the instrumental resolution of 0.3 meV. The resulting profile, not shown here, exhibits a large structured peak at around -5 meV and is not noticeably different from the low-temperature spectrum. The second situation describes the 45-K scattering spectrum for an effective $2 \times \infty$ Ar layer [Fig. 6(b)]. A full dynamical calculation of such a structure would be prohibitively expensive, so we have simulated a disorder along the x axis of MgO for the argon atoms starting from the 2×3 structure. The four perpendicular frequencies of the 2×3 cell are then replaced by the average frequency $\bar{\omega}$ and the frequency distribution around $\bar{\omega}$ is described by a Gaussian function with a FWHM equal to the frequency difference between the minimum and maximum frequencies of the perpendicular modes in the 2×3 cell. This spectrum with unchanged vibrations along the y axis is then convoluted with the instrumental resolution $\delta E = 0.3E'_N/5$ meV [Fig. 6(b)], where E'_N is the scattered neutron energy. The resulting shapes exhibit a single large peak around -5 meV instead of the structured peak associated with the 2×3 structure. The comparison with INS data at $T = 45$ K and 0.8 ML [Fig. 6(a)] shows that the main experimental energy gain peak at about 4 meV is structureless, which is in agreement with the features exhibited by the calculated neutron spectrum for the $2 \times \infty$ structure of the disordered high-temperature phase at 0.8 ML coverage.

The INS spectrum of the hexagonal incommensurate Ar layer has also been calculated [Figs. 3(b) and 5(b)]. The bar spectrum, without instrumental broadening, exhibits a single peak with a weak intensity structure between -3 and -1 meV. The peak located around -3.8 meV is due to the perpendicular vibrations of the monolayer atoms. Owing to incommensurability, the atom sites are all different and a frequency dispersion is calculated which has a Gaussian shape with a FWHM of about 0.2 meV. This spectrum is broadened by the instrumental line shape (FWHM ~ 0.3 eV) and it exhibits [Fig. 5(b)] a main peak at 3.8 meV with additional wings. This result is in good agreement with the structure in the experimental spectrum taken at $T = 10$ K and 1.16 ML, located in the loss spectrum at around 4 meV [Fig. 3(a)]. This energy is smaller than the one calculated for the 2×3 structure (~ 5 meV), a feature which is in semiquantitative agreement with experiments. On the other side, the gain spectrum does not display any structure at $T = 10$ K. In contrast, at $T = 45$ K, the calculated spectrum [Fig. 5(b)] exhibits gain and loss peaks whose intensities are proportional to the phonon annihilation or creation process ratio and the comparison with the experimental gain spectrum at $T = 45$ K and 1.16 ML [Fig. 5(a)] is satisfactory as far as the measured gain side is concerned.

C. Discussion

The above comparison shows that QENS and INS spectra exhibit significant differences depending upon the adlayer geometry. Diffusion and long-range order measurements indicate a unidirectional mobility which is along a Mg row, as shown by calculations for the $2 \times \infty$ structure; the calculated value of the diffusion constant D_x along this direction is relatively close to the estimated experimental value if we consider that D depends exponentially on the barrier height determining the frequency jump for the argon atoms. The smaller calculated value for D_x means that this potential barrier is probably slightly overestimated in our model. In the experiment performed on 1.16 layer, the observed mobility appears to be associated with the second layer atoms which can diffuse easily. Data obtained from QENS thus gives information on the MgO corrugation experienced by Ar atoms along Mg rows.

The main peaks in the calculated INS spectra of the 2×3 and hexagonal structures do not have the same shape: there is ill-resolved structure in the case of the 2×3 layer but a single broad peak for the hexagonal layer. The structured peak at $T = 10$ K is interpreted as the signature of the perpendicular vibrations of the four atoms in the 2×3 primitive cell. The present experiment confirms such an interpretation based on intermolecular potential calculations. In contrast, the single broad peak of the hexagonal structure or of the $2 \times \infty$ structure at 45 K corresponds rather to a range of perpendicular vibrational frequencies for the atoms, as expected for incommensurate or partly disordered phases. The energies of the two main peaks are larger for the commensurate structure; this is in qualitative agreement with the calcu-

lations. Finally, the secondary structures at lower energies seem to be more intense for the commensurate than for the incommensurate phase (with a maximum occurring in the 2×3 structure). These secondary structures are directly related to the barrier hindering the lateral motion of the layer which is responsible for the energy gap in acoustic dispersion curves.

An overestimate of the force constants for the atom-surface and atom-atom binding leads to energies for the main peaks which are overestimated by 20% for the 2×3 structure. This discrepancy between the observed and calculated density of states strictly suggests a shortcoming of the LJ potential reflected in the second derivative. In particular, additional contributions to the interaction potentials such as the influence of MgO rumpling can be responsible for changes in the curvature of the potential surface. It is expected that the perpendicular frequencies would be more sensitive to the softening of the force constants of commensurate phases than incommensurate phases. But more probably, this is also due to the failure of the present dynamical harmonic model to predict the frequencies of the perpendicular motions of the layer atoms. Anharmonicity[22] would reduce such frequencies and introduce a slight temperature dependence which has been noted in experiments.

It is interesting to compare the INS spectra of incommensurate phases of Ar adsorbed on MgO and on graphite.[24,25] For graphite, three peaks are observed; two are located at about 3.5 meV and 5.5 meV and the third, characterizing the out-of-plane (perpendicular) response, lies between 5 and 6 meV.[24] The relative intensity of these peaks fundamentally depends on the **Q**-vector orientation,[22,24] and it is shown that, in the INS spectrum of the Ar/Gr system, the transverse and longitudinal in-plane modes have significantly larger weights than the out-of-plane one. In the present results on Ar/MgO, the average over the **Q** orientations tends to favor the out-of-plane response in the INS spectrum.

V. CONCLUSION

A simultaneous experimental and theoretical study of quasielastic neutron-scattering and inelastic neutron-scattering spectra of an Ar monolayer adsorbed on MgO(100) has been performed in order to provide information on the layer dynamics. The physical quantities which are implicated in QENS and INS are, respectively, the pair-correlation function of monolayer atoms leading to the interpretation of the layer diffusion mechanism, and the second derivatives of the interaction potential (layer-layer and layer-substrate force constants). It has been shown that we can interpret in a satisfactory way the proposed unidirectional layer mobility and the shape of the INS spectra by focusing more deeply on the differences between two layer geometries: the 2×3 commensurate phase and the hexagonal incommensurate phase which occur successively when the Ar coverage is increased. Hence the experimental results prove to be a good test of the quality of the Ar/MgO(100) interaction potential proposed previously.[8,9,26] However, these experimental results suffer from a poor signal-to-noise ratio which does not allow us to resolve the three peaks expected at ~ -5 meV for the 2×3 structure. New experiments on neutron inelastic instruments providing a larger flux would certainly improve the quality of the data and would probably distinguish between these peaks.

ACKNOWLEDGMENTS

The authors wish to acknowledge Dr. A. J. Stone (Cambridge University) for improving the text. Faculté des Sciences de Luminy is "Associé aux Universités d'Aix–Marseille 2 et 3." The Laboratoire de Physique Moléculaire is "Unité Associée au Centre National de la Recherche Scientifique No. 772." The Faculté des Sciences de Luminy and Laboratoire Léon Brillouin are Unités Associées au Centre National de la Recherche Scientifique.

[1] *Phase Transitions in Surface Films 1*, edited by J. G. Dash *et al.* (Plenum, New York, 1980).
[2] *Phase Transitions in Surface Films 2*, edited by H. Taub *et al.* (Plenum, New York, 1991).
[3] T. Meichel, J. Suzanne, and J. M. Gay, C. R. Acad. Sci. Paris **11**, 989 (1988).
[4] T. Meichel, J. Suzanne, C. Girard, and C. Girardet, Phys. Rev. **38**, 3781 (1988).
[5] J. P. Coulomb, in *Phase Transitions in Surface Films 2* (Ref. 2), p. 113.
[6] J. P. Coulomb, M. Bienfait, and P. Thorel. J. Phys. **42**, 283 (1981), and references therein.
[7] M. Bienfait and J. M. Gay, in *Phase Transitions in Surface Films 2* (Ref. 2), p. 307.
[8] C. Girardet and C. Girard, Phys. Rev. B **39**, 8643 (1989).
[9] C. Ramseyer, P. N. M. Hoang, and C. Girardet, Surf. Sci. **265**, 293 (1992).
[10] G. Dolling, in *Lattice Dynamics and Intermolecular Forces*, edited by S. Califano (Academic Press, New York, 1975), p. 176.
[11] A. A. Maradudin, E. W. Montroll, G. H. Weiss, and I. P. Ipatova, in *Theory of Lattice Dynamics in the Harmonic Approximation* (Academic Press, New York, 1971).
[12] P. G. de Gennes, Physica **25**, 825 (1959).
[13] K. Sköld, Phys. Rev. Lett. **19**, 1023 (1967).
[14] B. A. Dasannacharya and K. R. Rao, Phys. Rev. **137**, A417 (1965).
[15] M. Bee, in *Quasi-elastic Neutron Scattering* (Hilger, Bristol, 1988).
[16] J. Ma, D. L. Kingsbury, F. C. Liu, and O. E. Vilches, Phys. Rev. Lett. **61**, 2348 (1988).
[17] M. Bienfait, J. M. Gay, and H. Blank, Surf. Sci. **204**, 331 (1988).
[18] P. Zeppenfeld, M. Bienfait, F. C. Liu, O. E. Vilches, and G. Coddens, J. Phys. **51**, 1929 (1990).
[19] M. Maruyama, M. Bienfait, F. C. Liu, Y. M. Liu, O. E. Vilches, and F. Rieutord, Surf. Sci. **283**, 223 (1993).
[20] J. M. Layet, M. Bienfait, and F. Rieutord, C. R. Acad. Sci.

Paris **313**, 319 (1991).
[21] A. Lakhlifi and C. Girardet, J. Chem. Phys. **94**, 688 (1991).
[22] T. M. Hakim and M. R. Glyde, Phys. Rev. **B 41**, 1640 (1990).
[23] C. Girardet and P. N. M. Hoang, Surf. Sci. **282**, 288 (1992).
[24] H. Taub *et al.*, Phys. Rev. Lett **34**, 654 (1975); Phys. Rev. **16**, 4551 (1977).
[25] C. Tiby and H. J. Lauter, Surf. Sci. **117**, 277 (1982).
[26] G. Vidali, G. Ihm, H. Y. Kim, and M. W. Cole, Surf. Sci. Rep. **12**, 133 (1991).

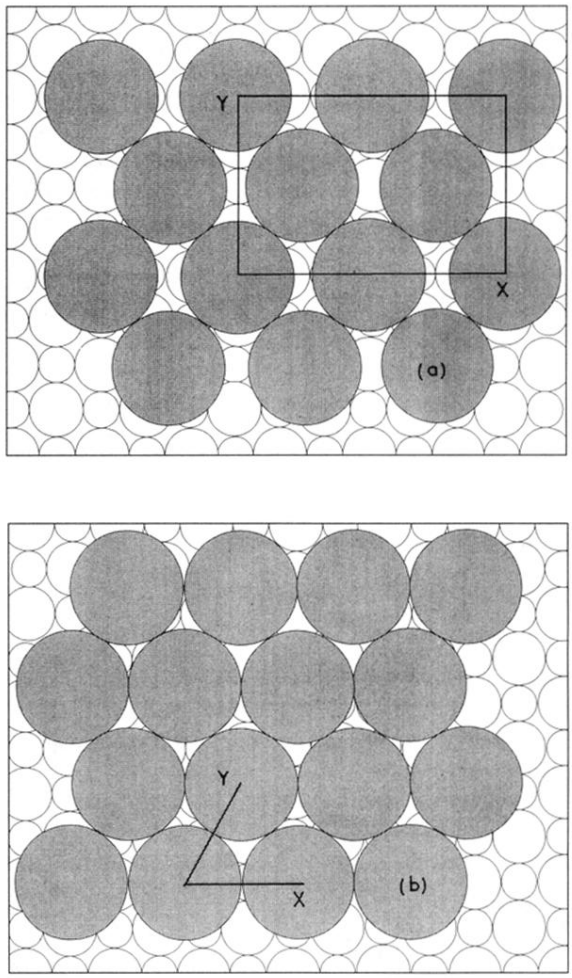

FIG. 1. The low-temperature (10 K) structures of Ar overlayer adsorbed on MgO(100). (a) The partially commensurate rectangular 2×3 solid at intermediate coverages (0.7–0.95 layer); (b) the hexagonal close-packed structure at monolayer completion.